A machining test to identify rotary axis geometric errors on a five-axis machine tool with a swiveling rotary table for turning operations

Soichi Ibaraki[a], Ibuki Yoshida[b], Tetsushi Asano[b]

[a]*Department of Mechanical Systems Engineering, Hiroshima University*
Kagamiyama 1-4-1, Higashi Hiroshima, 739-8527, Japan. Phone/Fax: +81-82-424-7580
[b]*Kawasaki Heavy Industries, Ltd.*
Kawasaki-cho 1-1, Akashi, 673-8666, Japan.

Type of contribution: Original research paper

Abstract

Lately, a cylindrical workpiece of relatively large diameter is often machined by turning operations by a swiveling rotary table in a five-axis machining center. This paper presents a machining test containing features finished by a turning operation by a swiveling rotary table. Unlike conventional machining tests for turning operations described in ISO 13041-6:2009, the present machining test can identify a complete set of position and orientation errors of the axis average line of rotary axes from the geometry of the finished test piece. The radial and axial error motions of the rotary table can be also observed when the swiveling axis is positioned horizontal ($A = 0°$) and vertical ($A = -90°$). Experimental demonstration is presented. The rotary axis geometric errors identified from the finished test piece's geometry are compared with those estimated by a conventional error calibration test using

Email address: ibaraki@hiroshima-u.ac.jp (Soichi Ibaraki)

a touch-triggered probe and a precision sphere. The uncertainty analysis for the present machining test is also presented.
Keywords: five-axis machine tool, machining test, turning, error calibration, geometric error

---

1. Introduction

Conventionally, a cylindrical workpiece of relatively large diameter is machined by turning operations on a large vertical-type numerically controlled lathe. Lately, such a large cylindrical workpiece is often machined by turning operations by a swiveling rotary table on a five-axis machining center (see Fig. 1 for an example machine configuration). Typical examples of such a workpiece include a cylindrical casing part in an aircraft jet turbine engine (e.g. Rolls-Royce[1]). Its machining process can be described as follows:

- Its cylindrical faces and flanges are finished by turning operations.
- It has many holes. Some are in the axial direction and others are in the radial direction.
- It also has features on flanges that are finished by end milling operations from either axial or radial direction.

It does not require simultaneous five-axis operation. To minimize the influence of the machine's error motions, the manufacturer often prefers "3+2 axis machining", where each feature is machined with the workpiece (or the tool) fixed at a limited set of angular positions – typically only in vertical ($A = 0°$) and horizontal ($A = -90°$) directions. By machining it on a five-axis machining center with a swiveling rotary table of the capability of turning operations, the machining time and cost can be significantly reduced, compared to conventional processes using both a vertical-type lathe and a machining center.

For example, the position tolerance for holes on a jet engine casing part is

typically below 50 μm. The workpiece's diameter is typically up to 1.5 m. For such a machining operation, one of major error contributors is quasi-static position and orientation errors of rotary axis average lines (the mean location of the axis of rotation is referred to as *the axis average line* in ISO 230-1 [2]). They are typically caused by the assembly error by a machine tool builder, but they can significantly change in a machine user's site due to environmental influence, or long-term performance deterioration ("aging") [4, 5, 6]. To maintain the finished workpiece's geometric accuracy within the given tolerance, it is important for a machine tool user to periodically perform the calibration of rotary axis geometric errors and then compensate for them.

Numerous error calibrations schemes for five-axis machines have been presented in literature. Their good review is in [7, 8]. ISO 10791-1 [9] was revised in 2015 with quasi-static tests for rotary axes. ISO 10791-6 [10] was revised in 2014 with dynamic interpolation tests for rotary axes. Although it is important to evaluate rotary axis geometric errors by such a non-cutting test, typical machine tool users consider more the machine's accuracy when it performs actual machining. Non-cutting tests are sometimes performed when the machine is "cold" without sufficient machine warm-up. In normal operating conditions with spindle rotation, the machine's geometric errors may be significantly different. For this reason, a machining test is often considered crucial to evaluate a machine's actual performance. ISO 10791-7 [11], revised in 2015, contains two machining tests for a five-axis machine tool. The cone frustum machining test was first presented in NAS979 [12] and is now adopted in [11]. Many researchers presented its analysis [13, 14] and clarified that it is difficult, or not possible, to separately diagnose error

causes from the geometric error of the finished test piece. Many five-axis machining tests proposed in the literature can be seen as a non-diagnostic test, e.g. the S-curve test [15], the NCG recommendation 2005 [16], the truncated square pyramid test [17], and the ball end milling test of hemisphere [18]. Refs. [19, 8] presented more thorough review.

On the other hand, simpler cutting tests, e.g., a planar grinding test [20], a grooving test by a single-point cutting tool [21], can be used to calibrate the position of rotary axis average lines. In [6, 19], a part of the authors proposed the pyramid-shaped machining test such that all position and orientation errors of rotary axis average lines can be separately identified by evaluating the finished test piece's geometric error. Similarly, some researchers presented machining tests to indirectly assess the machine's geometric errors. Velenosi et al. [22] presented the test analogous to the one in [6]. The test M4 in ISO 10791-7 [11] can be seen as a sub-set of the test in [6]. Morimoto et al. [23] presented a machining test by a non-rotating tool to calibrate a part of rotary axis location errors.

The machining tests reviewed above are mostly for milling operations. In turning operations, a motor for a rotary table generates the heat. The objective of this paper is to propose a machining test for turning operations by a swiveling rotary table such that machine geometric errors can be observed under the thermal influence of table rotation. To our knowledge, machining tests for turning operations are only presented in ISO 13041-6 [24] (for turning machines and turning centres), and ISO 1708 [25] (for general-purpose lathes). These tests only check a main workholding spindle, and the geometry of the finished test piece is influenced only by its radial and axial error

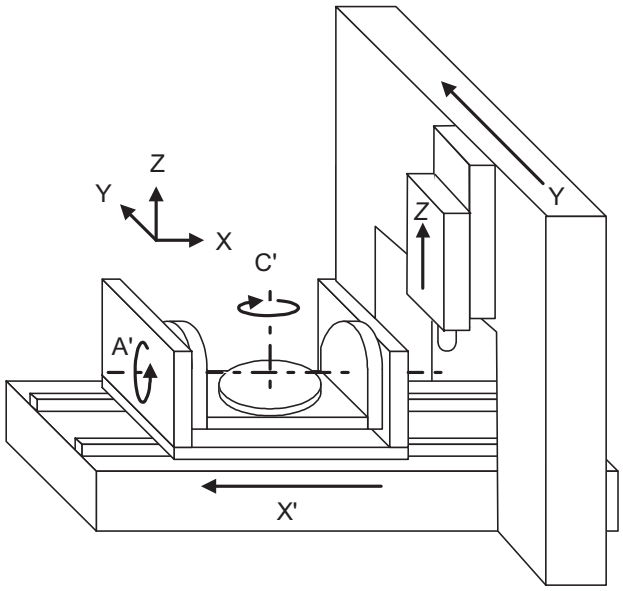

Figure 1: Machine configuration.

motions.

Compared to these conventional tests, the novelty of the machining test proposed in this paper can be summarized as follows: 1) a complete set of position and orientation errors of the axis average line of two rotary axes can be identified from the geometry of the finished test piece. 2) Error motions of a rotary table may vary with the angular position of its swiveling axis due to e.g. the gravity-induced deformation of machine structure or bearings. They can be assessed from the geometry of the finished test piece when the swivelling axis is positioned horizontal ($A = 0°$) and vertical ($A = -90°$). 3) The squareness errors of linear axes can be also identified.

2. Proposed machining test

2.1. Machining procedure

The target machine is a five-axis machine tool that performs turning operations using a swiveling rotary table, with angular discrete indexing of a workpiece at $A = 0^\circ$ (horizontal) and $A = -90^\circ$ (vertical) (continuous five-axis contouring is out of this paper's focus). The paper's basic idea can be exteded to other five-axis machine configurations, e.g. a rotary table and a spindle with one swivel axis.

Figure 2 shows the nominal geometry of the finished test piece. The dimensions are examples only; they can be modified according to e.g. the machine's table size (see Remark #3). This paper considers a five-axis machine shown in Fig. 1 with two rotary axes in the workpiece side. The finishing procedure is as follows:

1. *Reference circular groove:* Its cylindrical inner side face is shown by S_R and its bottom face is shown by B_R in Fig. 2. At $A = C = 0^\circ$, it is end-milled by driving X- and Y-axes along a circular path, centered at the origin of the machine coordinate system (MCS). The MCS is a fixed coordinate system with its origin at the intersection of nominal A- and C-axis centerlines (see ISO 230-1 [2], Annex A).
2. *Holes, H_1 to H_{16}:* at $A = C = 0^\circ$, the hole H_1 is finished at $(X, Y) = (140, 0)$ mm in the MCS. By indexing the C-axis at every 22.5°, total 16 holes, H_1 to H_{16}, are finished at the same position in the MCS.
3. *Turning of S_1 and B_1:* At $A = 0^\circ$, rotate the test piece in a constant speed by the C-axis. At $Y = 0$, feed the tool to -X direction toward $X = r_1$ to turn the bottom faces, B_1, where r_1 is the nominal radius

of the face S_1 ($r_1 = 160$ mm in Fig. 2). The machine setup is shown in Fig. 3a. Similarly, feed the tool to -Z direction toward $Z = z_1$ to turn the side faces, S_1, where z_1 is the nominal Z position of the face B_1 .

4. *Turning of S_4 and B_4:* The side face, S_4, and the bottom face, B_4, are turned similarly at lower $Z = z_4$,. Its setup is shown also in Fig. 3a.
5. *Turning of S_2 and B_2:* The side face, B_2 is turned at $X = 0$ by feeding the tool to -Y direction toward $Y = r_2$, where $r_2 = 165$ mm in Fig. 2. Its setup is also shown in Fig. 3a. The bottom face, B_2 is turned similarly.
6. *Turning of S_5 and B_5:* The faces, S_5 and B_5 are turned similarly as S_2 and B_2 at lower $Z = z_5$. Its setup is shown also Fig. 3a.
7. *Turning of S_3 and B_3:* Index the A-axis at $A = -90°$. At $X = 0$, feed the tool to -Z direction toward $Z = r_3$ to turn the bottom face B_3, where r_3 is the nominal radius of the face S_3 ($r_3 = 170$ mm in Fig. 2). Its setup is shown in Fig. 3b. The side face, S_3, is turned by feeding the tool to +Y direction.
8. *Turning of S_6 and B_6:* At $A = -90°$, the side face, S_6, and the bottom face, B_6, are turned similarly as S_3 and B_3. Its setup is shown also in Fig. 3b.

Remark #1: The machining conditions, e,g. the feed speed, the C-axis rotation speed, the depths of cut, should be chosen properly such that 1) the surface finish is good enough not to disturb the CMM measurement, and 2) the influence of cutting forces on the finished test piece's geometry can be minimized. ISO 230-1 [2] (Annex B) states that "machining tests related to a machine tool's quasi-static geometric accuracy should be performed as the

machine tool moves slowly and behaves in a quasi-static manner, i.e. with no dynamic influences and servo control limitations. The machine tool should not be influenced by any significant machining forces." It is assumed that the influence of cutting vibration, servo control dynamic errors, and tool wear is suffciently small. It is also noted that the test piece's setup error does not affect the test result, as long as it is sufficiently small not to significantly influence the actual depth of cut in the finishing process.

Remark #2: The number of the holes in Step 2 (16 in Fig. 2) should be designed according to the expected radial error motion of C-axis. If the number of the holes is too few, larger radial error motion may significantly influence the calculated concentricity of the pitch circle of the holes (#1 in Table 1).

Remark #3: In principle, the size of the test piece should be in accordance with typical uses for the machine tool under test. The weight of the test piece may change rotary axis geometric errors particularly at $A = -90°$. When the test piece is smaller, the surface roughness of the machined surface may give larger uncertainty for the parallelism error, i.e. #2 in Table 1, but other errors are less influenced in principle by the size of the test piece. When the test piece is larger, the CMM measurement uncertainty can be larger. The influence of linear axis error motions, which are not included in Table 2, can be also larger.

2.2. Measurement

Table 1 shows geometric errors of the finished test piece that should be measured by using a coordinate measuring machine (CMM). The definition of geometric errors is in accordance with ISO 1101 [27]. The measurement

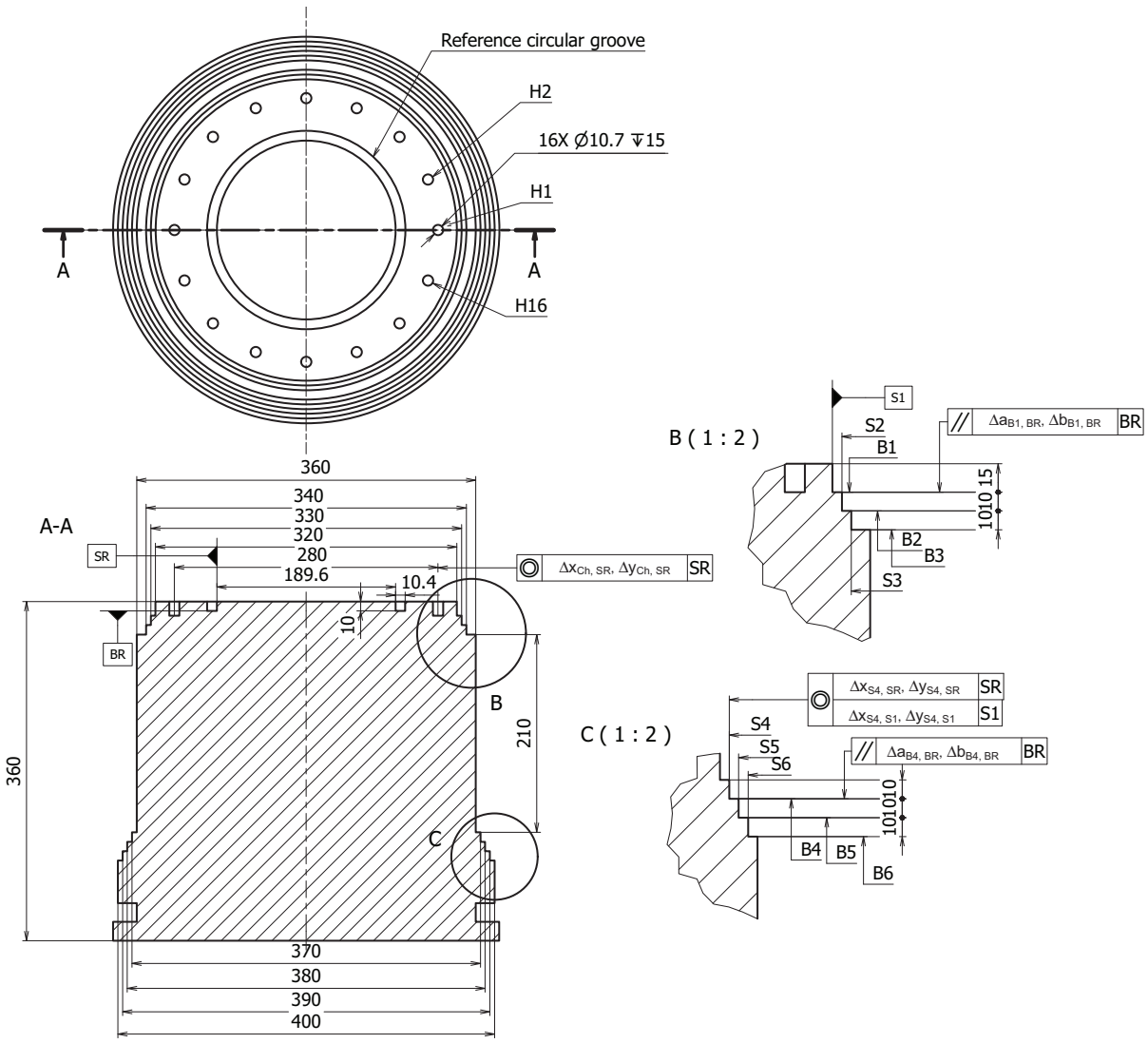

Figure 2: Nominal test piece geometry. The geometric errors are shown by the GD&T (geometric dimensioning and tolerancing) tolerance symbol in ISO 1101 [27]. See Table 1 for their definition.

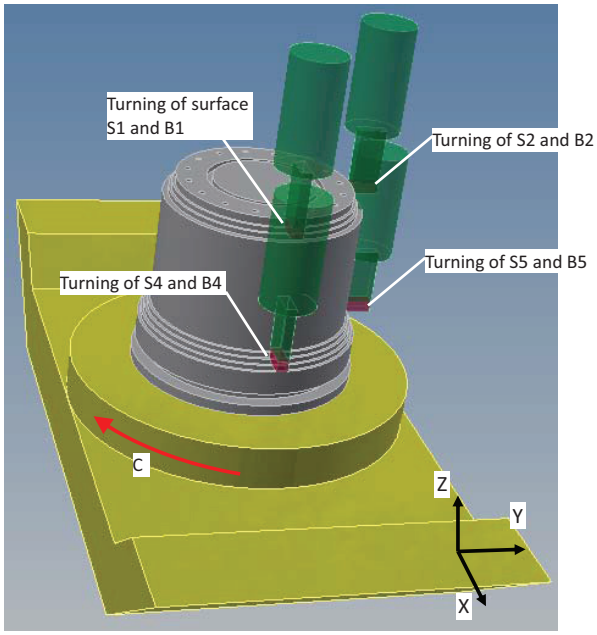

a)

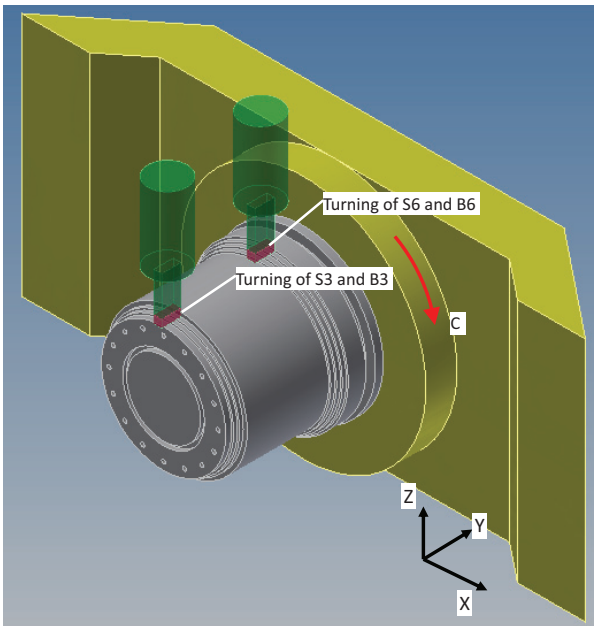

b)

Figure 3: Machining procedure. a) at $A = 0°$, b) at $A = -90°$.

coordinate system is defined as follows: its origin (X,Y) is defined at the center of the best-fit circle to probed points on the reference circular groove's side face, S_R. Its Z origin is defined at the Z-position of the plane best-fit to probed points on the reference circular groove's bottom face, B_R. The orientation of the X-axis is defined by a line connecting this origin and the best-fit center of the hole H_1. The orientation of the Y-axis around the X-axis is defined from the origin and the face B_R.

The circularity profile of side circular faces, S_i $(i = 1, 3, 4, 6)$, denoted by $\Delta r_{S_i}(C)$ (items a to d in Table 2), is defined as the deviation of the measured profile from its best-fit circle. "(C)" represents a profile as a function of the C-axis angular position, C.

Remark: in the GD&T symbols defined in [27], concentricity and parallelism errors are defined by a single value describing the size of the tolerance zone. In this paper, they are defined in two directions.

3. Identification of machine tool geometric errors

3.1. Machine geometric errors to be identified

Table 2 shows machine tool geometric errors that can be identified from the geometric error of the finished test piece. At $A = 0°$, $(\delta x_{CR}(0°), \delta y_{CR}(0°))$ represents position errors of the C-axis average line from its nominal position in X- and Y-directions. $(\alpha_{CR}(0°), \beta_{CR}(0°))$ represents orientation errors of the C-axis average line around X- and Y-axes of the machine coordinate system. The subscript, "CR", represents the error of the C-axis with respect to the machine coordinate system ("R" for the reference).

At $A = -90°$, the position error of C-axis is parameterized by the position

Table 1: Geometric errors of the finished test piece and their causes. The column "Measured on finished test piece" shows measured errors of the finished test piece in the experiment to be presented in Section 4.

#	Geometric error	Symbol	Major causes	Measured on finished test piece
1	Concentricity of the pitch circle of holes, C_h, to S_R	$\Delta x_{C_h,S_R}$ in X $\Delta y_{C_h,S_R}$ in Y	Position error of C-axis at $A = 0°$ and $Z = z_h$	10.1 μm -17.2 μm
2	Parallelism of B_1 to B_R	$\Delta a_{B_1,B_R}$ around X $\Delta b_{B_1,B_R}$ around Y	C-Y squareness error at $A = 0°$ C-X squareness error at $A = 0°$	-8.7 μrad 1.7 μrad
3	Error in distance between B_3 and B_R	$\Delta d_{B_3,B_R}$	Position error of A-axis in Y Position error of A-axis in Z	23.0 μm
4	Error in diameter of S_3	Δr_{S_3}	Position error in Z of C-axis at $A = -90°$	-14.5 μm
5	Concentricity of S_4 to S_R	$\Delta x_{S_4,S_R}$ in X $\Delta y_{S_4,S_R}$ in Y	Position error of C-axis at $A = 0°$ and $Z = z_4$	12.9 μm -23.3 μm
6	Concentricity of S_4 to S_1	$\Delta x_{S_4,S_1}$ in X $\Delta y_{S_4,S_1}$ in Y	C-Z parallelism around Y C-Z parallelism around X	-1.2 μm -0.7 μm
7	Concentricity of S_6 to S_3	$\Delta x_{S_6,S_3}$ in X $\Delta y_{S_6,S_3}$ in Y	C-Y parallelism around Z at $A = -90°$ C-Y parallelism around X at $A = -90°$	-0.3 μm -2.2 μm
a	Circularity profile of S_1	$\Delta r_{S_1}(C)$	Radial and tilt error motions of C-axis at $A = 0°$	See Fig. 8a.
b	Circularity profile of S_3	$\Delta r_{S_3}(C)$	Radial and tilt error motions of C-axis at $A = -90°$	See Fig. 8b.
c	Circularity profile of S_4	$\Delta r_{S_4}(C)$	Radial and tilt error motions of C-axis at $A = 0°$	See Fig. 8a.
d	Circularity profile of S_6	$\Delta r_{S_6}(C)$	Radial and tilt error motions of C-axis at $A = -90°$	See Fig. 8b.

error of A-axis, $(\delta y_{AR}(-90^\circ), \delta z_{AR}(-90^\circ))$, and the intersection error of C- to A-axis, $\delta y_{CA}(-90^\circ)$. Its orientation error is parameterized by $\alpha_{CR}(-90^\circ)$ around the X-axis and $\gamma_{CR}(-90^\circ)$ around the Z-axis.

Remark #1: In ISO 230-1 [2], position and orientation errors of the axis average line of a rotary axis, or "location errors" in ISO 230-7 [3], are defined as "mean" position and orientation errors over its entire angular work range. For example, when the squareness error of C- to A-axis average line differs at $A = 0^\circ$ and $A = -90^\circ$, the parameter $E_{B(0A)C}$, defined in ISO 230-1 [2], represents its mean value. Many previous works. e. g. [8, 13, 17, 22, 28] use this notation. This paper does not assume position and orientation errors of C-axis average line are the same at $A = 0^\circ$ and $A = -90^\circ$, and identify them separately. When they can be considered the same as the notation in ISO 230-1 [2], they can be converted as follows:

$$\delta x_{CR}(0^\circ) = E_{X0A} \tag{1}$$

$$\delta y_{CR}(0^\circ) = E_{Y0A} + E_{Y(0A)C} \tag{2}$$

$$\alpha_{CR}(0^\circ) = E_{A0A} \tag{3}$$

$$\beta_{CR}(0^\circ) = E_{B0A} + E_{B(0A)C} \tag{4}$$

$$\delta y_{AR}(-90^\circ) = E_{Y0A} \tag{5}$$

$$\delta z_{AR}(-90^\circ) = E_{Z0A} \tag{6}$$

$$\delta y_{CA}(-90^\circ) = E_{Y(0A)C} \tag{7}$$

$$\alpha_{CR}(-90^\circ) = E_{A0A} \tag{8}$$

$$\gamma_{CR}(-90^\circ) = E_{C0A} + E_{B(0A)C} \tag{9}$$

Table 2: Machine geometric errors to be identified by the proposed machining test. The column "Estimated from finished test piece" shows the values estimated from geometric errors of the finished test piece in the experiment in Section 4.3. The column "Estimated from probing test " shows the values estimated from the probing test presented in Section 4.4.

Symbol [29]	Description ("E_*" shows the corresponding symbol defined in ISO 230-1 [2]).	Estimated from finished test piece	Estimated from probing test
Position and orientation errors of C-axis average line at $A = 0°$			
$\delta x_{CR}(0°)$	Position error in X of C-axis at $A = 0°$	12.4 μm	-5.8 μm
$\delta y_{CR}(0°)$	Position error in Y of C-axis at $A = 0°$	-16.8 μm	-26.1 μm
$\alpha_{CR}(0°)$	Squareness error of C-axis to Y-axis at $A = 0°$	-8.7 μrad	-0.1 μrad
$\beta_{CR}(0°)$	Squareness error of C-axis X-axis at $A = 0°$	-7.0 μrad	5.2 μrad
Position errors of A-axis at $A = -90°$			
$\delta y_{AR}(-90°)$	Position error in Y of A-axis at $A = -90°$	36.5 μm	46.5 μm
$\delta z_{AR}(-90°)$	Position error in Z of A-axis at $A = -90°$	28.6 μm	18.7 μm
Position and orientation of C-axis average line at $A = -90°$			
$\delta y_{CA}(-90°)$	Intersection error of C- to A-axis	-25.4 μm	-31.6 μm
$\alpha_{CR}(-90°)$	Parallelism error of C-axis at $A = -90°$ to Y-axis around X-axis	36.7 μrad	47.1 μrad
$\gamma_{CR}(-90°)$	Parallelism error of C-axis at $A = -90°$ to Y-axis around Z-axis	1.6 μrad	2.4 μrad
Squareness errors of linear axes			
β^0_{ZX}	Squareness error of Z- to X-axis ($E_{B(0X)Z}$)	3.5 μrad	–
α^0_{ZY}	Squareness error of Z- to Y-axis ($E_{A(0Y)Z}$)	19.2 μrad	–
C-axis error motions. "(C)" represents a function of the C-axis angular position, C.			
$\Delta x_{CR}(C)(A = 0°)$	Radial error motion of C-axis at $A = 0°$ (E_{XC})	See Fig. 8a	–
$\beta_{CR}(C)(A = 0°)$	Tilt error motion of C-axis around Y at $A = 0°$ (E_{BC})	See Fig. 8a	–
$\alpha_{CR}(C)(A = 0°)$	Tilt error motion of C-axis around X at $A = 0°$ (E_{AC})	(from profiles of S_2 and S_5)	–
$\Delta z_{CR}(C)(A = -90°)$	Radial error motion of C-axis at $A = -90°$ (E_{YC})	See Fig. 8b	–
$\alpha_{CR}(C)(A = -90°)$	Tilt error motion of C-axis around X at $A = -90°$ (E_{AC})	See Fig. 8b	–

This paper uses this notation because the present test investigates rotary axis geometric errors only at $A = 0°$ and $A = -90°$, and there is no need to take their average.

Remark #2: Similarly, radial and tilt error motions of C-axis are also defined separately at $A = 0°$ and $A = -90°$, as shown in Table 2. C-axis error motions may vary due to e.g. the gravity-induced deformation of machine structure or bearings. This influence can be larger when the workpiece is heavier.

3.2. Identification of machine geometric errors

The five-axis kinematic model describes the TCP position in the workpiece coordinate system under machine geometric errors. It is the basis of the formulation presented in this subsection. It has been presented in many previous publications, e.g. [8, 28, 29] and thus is not presented here.

Position and orientation errors of C- and A-axis average lines: For example, Fig. 4 illustrates the influence of the position error C-axis at $A = 0°$, namely $\delta x_{CR}(0°)$ and $\delta y_{CR}(0°)$ (in Table 2), on the concentricity of the pitch circle of holes, C_h, to S_R, namely $\Delta y_{C_h,S_R}$ (#1 in Table 1). When $\beta_{CR}(0°) - \beta^0_{ZX}) = 0$, the difference between the C-axis position assumed in the CNC controller and its actual position moves the center of the pitch circle by $(\delta x_{CR}(0°), \delta y_{CR}(0°))$. When there exists the parallelism error of C- to Z-axis, the centerline position at $Z = z_h$ is displaced. Thus we have: #1: Concentricity of C_h to S_R

$$\Delta x_{C_h,S_R} = (\beta_{CR}(0°) - \beta^0_{ZX})z_h + \delta x_{CR}(0°) \quad (10)$$

$$\Delta y_{C_h,S_R} = -(\alpha_{CR}(0°) - \alpha^0_{ZY})z_h + \delta y_{CR}(0°) \quad (11)$$

Analogously, the geometric errors of the finished test piece shown in Table 1 are related to rotary and linear axis geometric errors shown in Table 2 in the following formulae:

#2: Parallelism of B_1 to B_R

$$\Delta a_{B_1,B_R} = \beta_{CR}(0^\circ) \tag{12}$$

$$\Delta b_{B_1,B_R} = \alpha_{CR}(0^\circ) \tag{13}$$

#3: Error in distance between B_3 and B_R

$$\Delta d_{B_3,B_R} = -\delta y_{AR}(-90^\circ) - \delta z_{AR}(-90^\circ) \tag{14}$$

#4: Error in diameter of S_3

$$\Delta r_{S_3} = -\delta z_{AR}(-90^\circ) - \delta y_{AR}(-90^\circ) - \delta y_{CA}(-90^\circ) + \alpha_{CY}(-90^\circ) z_3 \tag{15}$$

#5: Concentricity of S_4 to S_R

$$\Delta x_{S_4,S_R} = (\beta_{CR}(0^\circ) - \beta^0_{ZX}) z_4 + \delta x_{CR}(0^\circ) \tag{16}$$

$$\Delta y_{S_4,S_R} = -(\alpha_{CR}(0^\circ) - \alpha^0_{ZY}) z_4 + \delta y_{CR}(0^\circ) \tag{17}$$

#6: Concentricity of S_4 to S_1

$$\Delta x_{S_4,S_1} = \left(-\beta_{CR}(0^\circ) + \beta^0_{ZX}\right)(z_1 - z_4) \tag{18}$$

$$\Delta y_{S_4,S_1} = \left(\alpha_{CR}(0^\circ) - \alpha^0_{ZY}\right)(z_1 - z_4) \tag{19}$$

#7: Concentricity of S_6 to S_3

$$\Delta x_{S_6,S_3} = (-\gamma_{CR}(-90^\circ) + \gamma_{YX})(z_3 - z_6) \quad (20)$$

$$\Delta y_{S_6,S_3} = \alpha_{CR}(-90^\circ)(z_3 - z_6) \quad (21)$$

where z_i represents the nominal distance of the probed points on the face S_i in the Z-direction from the A-axis average line. z_h and z_R are respectively the nominal distance of the holes, H_i, and the reference circular groove's bottom face, B_R, in the Z-direction from the A-axis average line.

C-axis radial error motions: The C-axis radial error motion at $A = 0^\circ$, $\Delta x_{CR}(C)(A = 0^\circ), \Delta y_{CR}(C)(A = 0^\circ)$, and its tilt error motion, $\alpha_{CR}(C)(A = 0^\circ), \beta_{CR}(C)(A = 0^\circ)$, can be identified by solving the following equations:

$$\Delta r_{S_1}(C) = \Delta x_{CR}(C)(A = 0^\circ) + \beta_{CR}(C)(A = 0^\circ) \cdot z_1 \quad (22)$$

$$\Delta r_{S_2}(C + 90^\circ) = \Delta y_{CR}(C)(A = 0^\circ) - \alpha_{CR}(C)(A = 0^\circ) \cdot z_2 \quad (23)$$

$$\Delta r_{S_4}(C) = \Delta x_{CR}(C)(A = 0^\circ) + \beta_{CR}(C)(A = 0^\circ) \cdot z_4 \quad (24)$$

$$\Delta r_{S_5}(C + 90^\circ) = \Delta y_{CR}(C)(A = 0^\circ) - \alpha_{CR}(C)(A = 0^\circ) \cdot z_5 \quad (25)$$

The C-axis radial error motion $A = -90^\circ$, $\Delta z_{CR}(C)(A = -90^\circ)$, and its tilt error motion, $\alpha_{CR}(C)(A = -90^\circ)$, can be identified by:

$$\Delta r_{S_3}(C) = \Delta z_{CR}(C)(A = -90^\circ) + \alpha_{CA}(C)(A = -90^\circ) \cdot z_3 \quad (26)$$

$$\Delta r_{S_6}(C) = \Delta z_{CR}(C)(A = -90^\circ) + \alpha_{CA}(C)(A = -90^\circ) \cdot z_6 \quad (27)$$

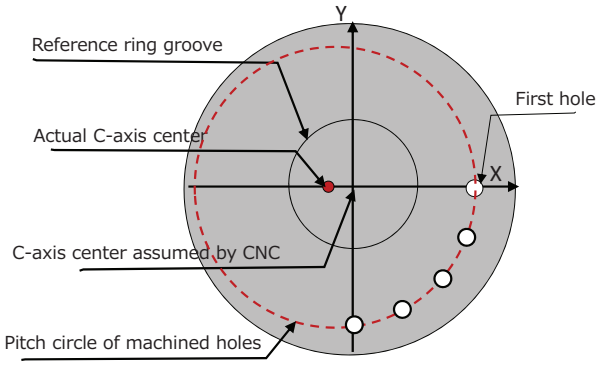

Figure 4: Influence of the position error C-axis at $A = 0°$, namely $\delta x_{CR}(0°)$ and $\delta y_{CR}(0°)$, on the concentricity of the pitch circle of holes, C_h, to S_R, namely $\Delta y_{C_h,S_R}$.

4. Experiment

4.1. Machining test setup

The machine configuration is shown in Fig. 1. The experimental setup is shown in Fig. 5. The tool, the workpiece material, and turning conditions are shown in Table 3. The C-axis rotation speed is regulated such that the cutting speed becomes the value shown here. Additionally, the reference circular groove (faces S_R and B_R) were finished by a radius end mill (tool material: coated carbide, number of teeth: 4, diameter: 8 mm) with cutting speed: 100 m/min for the side face, and 62.8 m/min for the bottom face, feed per tooth: 0.019 mm/tooth for the side face, and 0.025 mm/tooth for the bottom face, cutting direction: down cut, cutting fluid: Emulsion. The holes, H_i ($i = 1, \cdots 16$), were finished by a reamer (tool material: carbide, number of teeth: 4, diameter: 10.7 mm) with cutting speed: 13.5 m/min, feed per tooth: 0.006 mm/tooth, cutting fluid: Emulsion.

On the machine table, the distance between the reference circular groove's

Table 3: Machining conditions for turning of cylindrical faces (S_1 to S_6 and B_1 to B_6 in Fig. 2).

Chip	Included angle	80° (positive relief angle)
	Material	carbide
	Nose radius	0.8 mm
Workpiece material		Aluminum alloy (JIS A5053)
Depth of cut		0.8 mm
Cutting speed		250 mm/min
Feed rate		0.2 mm/rev
Cutting fluid		Emulsion

bottom face, B_R, to the nominal A-axis centerline was $z_R = 405.702$ mm. Therefore, $z_1 = 400.702$, $z_3 = 380.702$, $z_4 = 160.702$, and $z_6 = 140.702$ (see Section 3.2 for their definitions).

4.2. Measured test piece geometry

On each face of the finished test piece, S_R, B_R, S_1 to S_6, and B_1 to B_6, total 16 points (at every 22.5°) are probed on a CMM. With good understanding of five-axis kinematics, many observations can be made:

Figure 6a shows measured hole positions, H_1 to H_{16}, on the XY plane. The error between nominal and measured hole positions is magnified 1,000 times, i.e. the error 50 μm is magnified to 50 mm in the plot (see "Error scale"). The holes' pitch circle has the concentricity error to the origin of the measurement coordinate system, in other words, the concentricity error to the datum face S_R, which is denoted by $(\Delta x_{C_h,S_R}, \Delta y_{C_h,S_R})$ in Table 1 #1. Figure 6a shows that $(\Delta x_{C_h,S_R}, \Delta y_{C_h,S_R}) = (10.1, -17.2)$ μm. This is mostly caused by the position error of C-axis average line at $A = 0°$. Its relationship

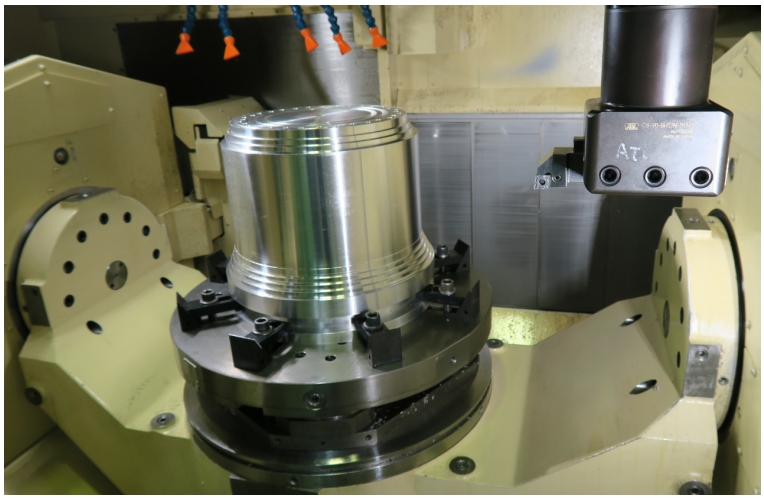

a)

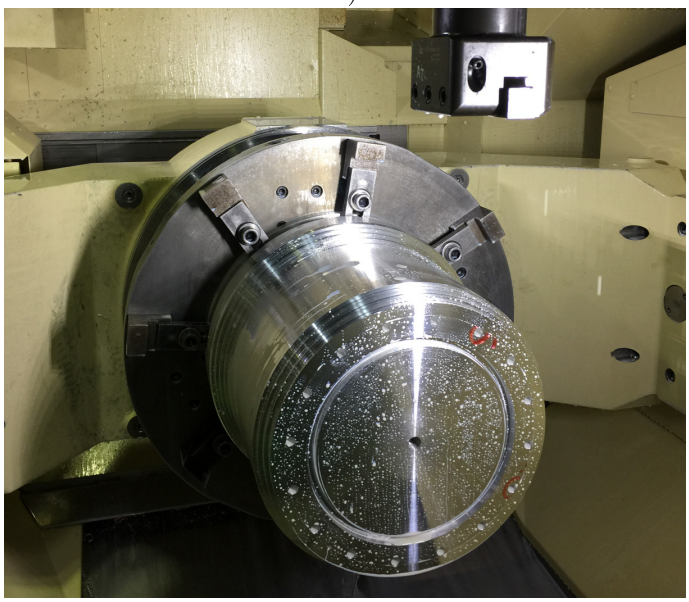

b)

Figure 5: Experimental setup. a) At $A = 0°$, b) at $A = -90°$.

is formulated in Eq. (10)(11).

Figure 6b shows measured points on the face B_1, projected onto the XZ plane. They show the parallelism error of B_1 to the datum surface B_R, $(\Delta a_{B1,BR}, \Delta b_{B1,BR}) = (-8.7, 1.7)$ μrad, as shown in Table 1 #2. This is caused by the squareness error of C-axis average line to X- and Y-axes, as is formulated in Eq. (12)(13).

Figure 6c shows measured points on the face B_3, projected onto the XZ plane. They show the error in distance between B_3 and B_R, $\Delta d_{B_3,B_R} = 23.0$ μm, as shown in Table 1 #3. It is caused by the position error of A-axis average line in both Y- and Z-directions, as is formulated in Eq. (14).

Figure 7a shows measured points on side faces S_1 and S_4, projected onto the XY plane. The concentricity error of S_4 to the origin is mostly caused by the position error of C-axis average line at $A = 0°$, as formulated in Eqs. (16)(17). On the other hand, the concentricity error of S_4 to S_1 represents the parallelism errors of C- to Z-axis, as formulated in Eqs. (18)(19) (In Eq. (18), notice that $\beta_{CR}(0°)$ represents the orientation error of C- to X-axis, and β^0_{ZX} represents that of Z- to X-axis. Therefore, their difference represents the parallelism error of C- to Z-axis around the Y-axis). Furthermore, the circularity profiles of S_1 and S_4 contain radial and tilt error motions of C-axis a $A = 0°$, as is formulated in Eqs. (22)(24).

Figure 7b shows measured points on side faces S_3 and S_6, turned at $A = -90°$. The error in the mean diameter of S_3 is mostly caused by the Z-position error of C-axis at $A = -90°$, and is formulated by Eq. (15). The concentricity error of S_6 to S_3 represents the parallelism error of C- to Y-axis at $A = -90°$ (see Eqs. (20)(21)). The circularity profiles of S_3 and S_6 repre-

sent radial and tilt error motions of C-axis at $A = -90°$ (see Eq. (26)(27)).

The column "Measured on finished test piece" in Table 1 shows measured geometric errors of the finished test piece, calculated from all the probed positions.

4.3. Identification of machine geometric errors

Position and orientation errors of rotary/linear axis average lines: The column "Estimated from finished test piece" in Table 2 shows the estimated position and orientation errors of rotary/linear axis average lines, identified by solving the equations presented in Section 3.2.

Error motions of C-axis: Figure 8 shows the circularity profiles measured on side faces a) S_1 and S_4, and b) S_3 and S_6. The circularity profile, $\Delta r_{S_i}(C)$ $(i = 1, 4, 3, 6)$, is the deviation of measured points, shown in Fig. 7, from its best-fit circle (see Section 3.2)..

The C-axis radial and tilt error motions at $A = 0°$ can be calculated from Fig. 8a by Eqs. (22)(23)(24)(25). The C-axis radial and tilt error motions at $A = -90°$ from Fig. 8b by Eqs. (26)(27). In all the faces shown in Fig. 8, the deviation is at most 3 μm and no significant radial and tilt error motion is observed.

4.4. Comparison with conventional non-cutting probing test

For experimental comparison, some parameters in Table 2 were identified by applying a conventional non-cutting test. As is reviewed in [8], many schemes have been studied to (semi-)automatically identify position and orientation errors of rotary axis average lines (location errors). The schemes using a touch-triggered probe are probably the most popular, since many

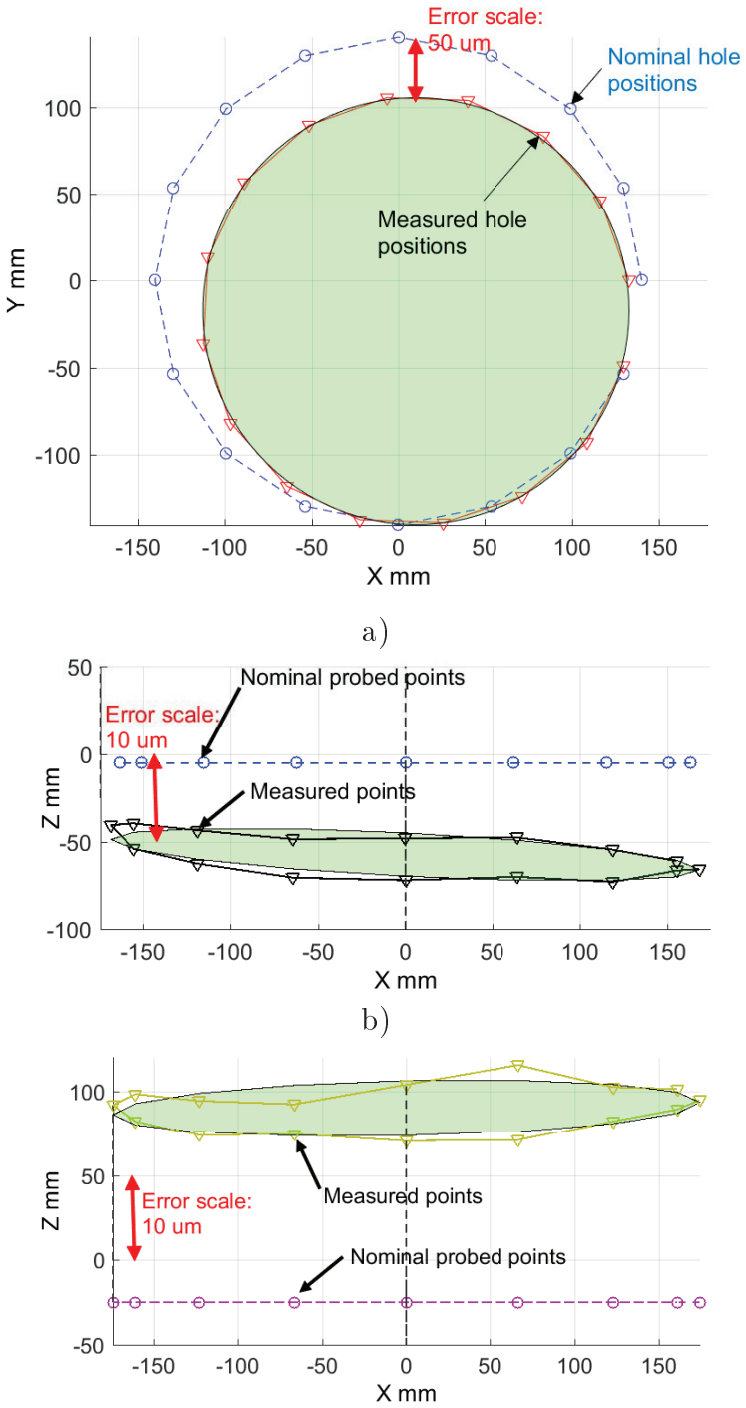

Figure 6: Geometric errors of the finished test piece measured by using a CMM. The error between nominal and measured points is magnified as shown by "Error scale." a) Measured hole positions, H_1 to H_{16}, on the XY plane. b) Measured points on the bottom face B_1, projected onto the XZ plane. c) Measured points on the bottom face B_3.

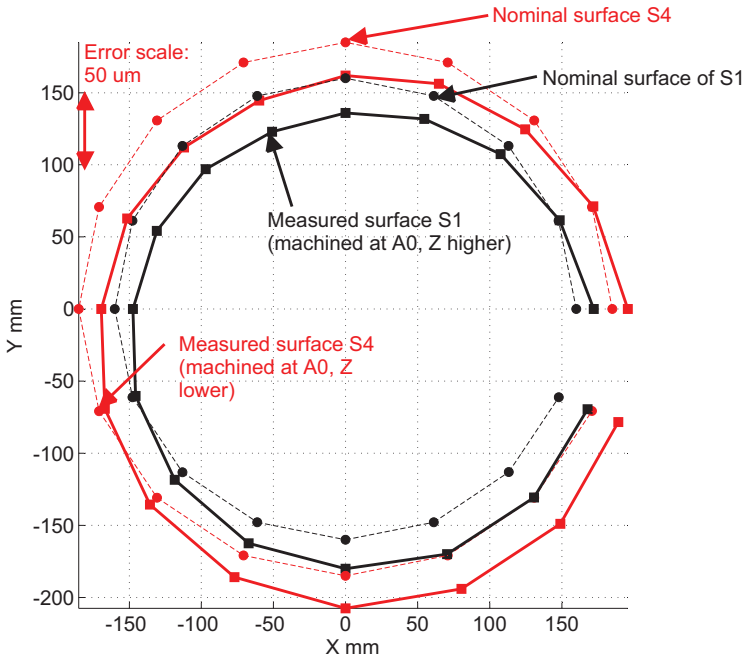

a)

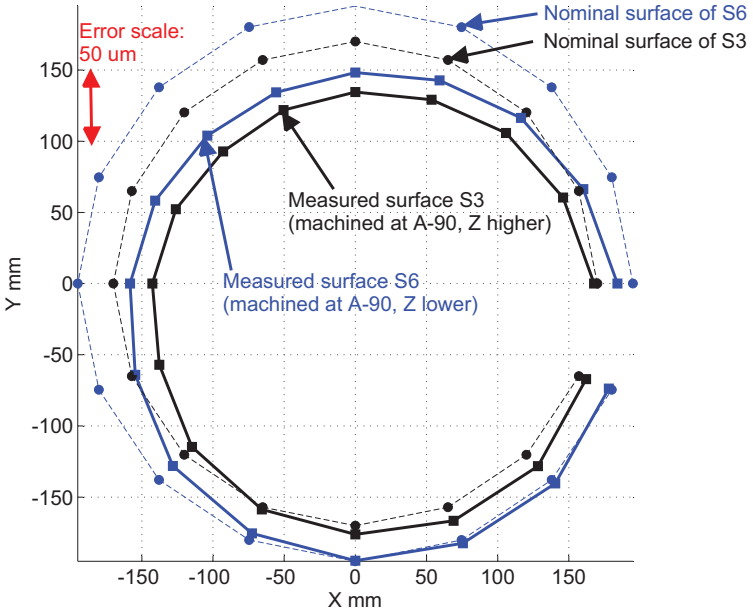

b)

Figure 7: Geometric errors of the finished test piece measured by using a CMM. a) Measured points on the side faces S_1 and S_4, projected onto the XY plane. b) Measured points on the side faces S_4 and S_6.

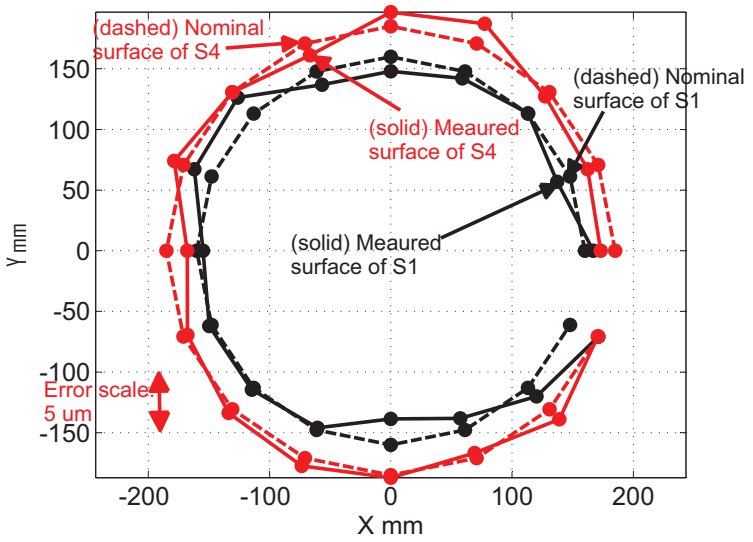

a)

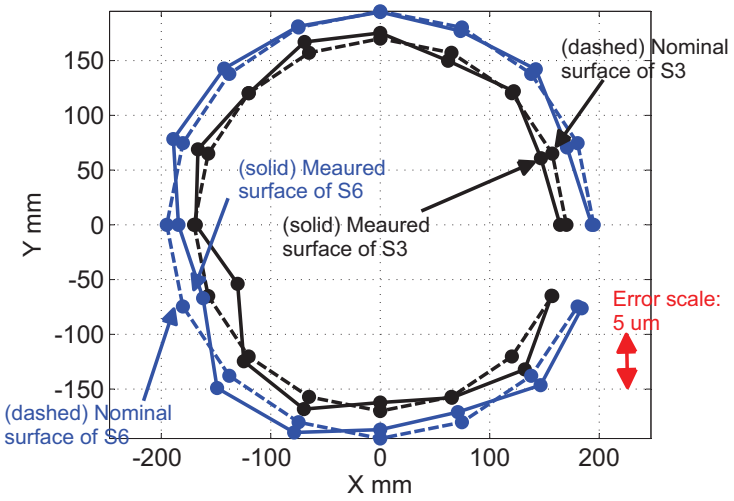

b)

Figure 8: The circularity profiles measured on side faces a) S_1 and S_4, and b) S_3 and S_6, projected onto the XY plane. The circularity profile is the deviation of measured points, shown in Fig. 6d) and e), from its best-fit circle. The error from the best-fit circle is magnified 10,000 times (see "Error scale"). a) The circularity profiles of S_1 and S_4. b) The circularity profiles of S_3 and S_6.

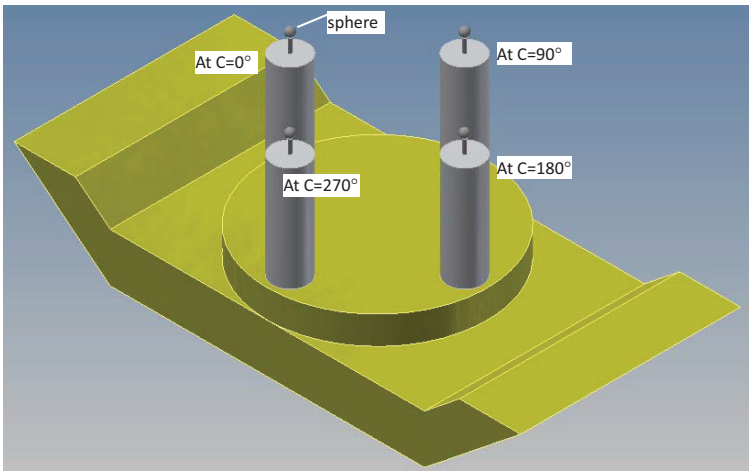

a)

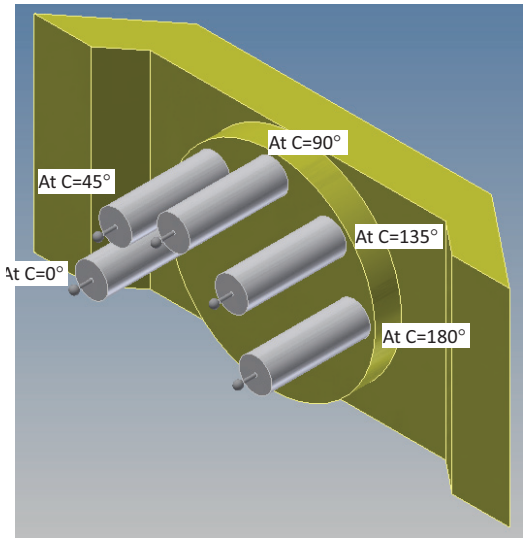

b)

Figure 9: Probing test setup. a) At $A = 0°$. b) $A = -90°$.

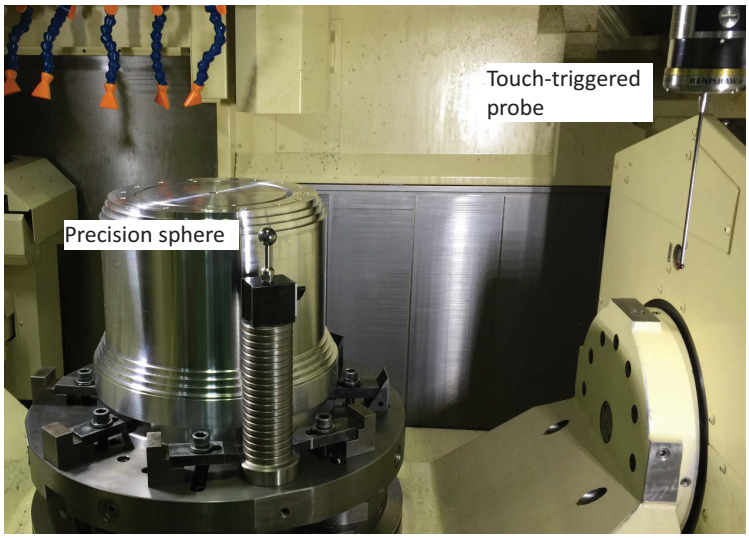

Figure 10: Probing test setup.

machine tools have it as a default on-machine measuring instrument. Many research works have been reported [30, 31, 32, 33, 34], and commercial products are available from several vendors.

Figure 9 illustrates the test procedure. A precision sphere is fixed on the machine table. At $A = 0°$, the C-axis is indexed at every 90° and the sphere center's three-dimensional position is measured by probing five points on its surface (see Fig. 9a). Analogously, at $A = -90°$, the sphere center's position is measured at $C = 0, 45, 90, 135, 180°$. This test is essentially the same as the R-test [35, 36]. The algorithm to identify rotary axis location errors in Table 2 from the R-test is presented in details in [37, 36].

Figure 10 shows the experimental setup. A precision sphere (ceramics, ϕ25 mm $\pm$1 μm) was fixed on the machine table near the finished test piece. A commercial touch-triggered probe, RMP600 by Renishaw (stylus ball: ϕ6.0

mm, stylus length: 200 mm, unidirectional repeatability: 0.35 μm (for stylus length 100 mm)), was used.

The column "Estimated from probing test" in Table 2 shows the identified rotary axis position and orientation errors. For most of position errors ($\delta y_{CR}(0^\circ)$, $\delta y_{AR}(-90^\circ)$, $\delta z_{AR}(-90^\circ)$, and δy^0_{CA})), the difference from the estimates by the finished test piece is within 10 μm. $\delta x_{CR}(0^\circ)$ has larger difference (about 18 μm). The maximum difference in estimated orientation errors was about 12 μrad (for $\beta_{CR}(0^\circ)$), which is not significant in this setup; its influence on the Z-displacement of the face B_1 is about 4 μm at maximum (the diameter of B_1 is 320 mm).

The difference can be due to the thermal influence. In the machining test, cutting fluid was used. Research works [38, 4] showed that cutting fluid can give significant influence on rotary axis position and orientation errors. A machining process can be influenced by many other factors, e.g. the heat generated by the rotary table's motor, the heat by the material removal process, and the influence of cutting force on e.g. tool deflection or surface roughness. The probing test is not influenced by them. The machine's geometric errors in actual machining processes may be observed better in the machining test.

The present experiments can compare both schemes only within each scheme's uncertainty. It cannot legitimately validate the present scheme's accuracy. The following section will present the uncertainty analysis for the proposed machining test.

5. Uncertainty analysis

5.1. Objective of uncertainty analysis

Major potential contributors to the uncertainty in the estimation of machine geometric errors in Table 2 by the proposed machining test are as follows:

1. *Unmodelled machine error motions:* Error motions of each linear axis, i.e. linear positioning, straightness and angular error motions, are ignored in this paper (only squareness errors of linear axes are considered), and thus they can be uncertainty contributors.
2. *Unrepeatable error motions of linear and rotary axes:* In addition to "random" error motions, the change in machine geometric errors during the machining process due to the thermal influence can be also an uncertainty contributor.
3. *Influence of machining process:* The machine's error motions may not be exactly copied to the finished test piece's geometry. The cutting force or the surface finish could influence test results.
4. *Measurement uncertainty of CMM:* Larger surface roughness could increase the CMM's measurement uncertainty.

The contributors 1 and 2 can be major uncertainty contributors for many "indirect" error calibration schemes proposed in past works. Researchers presented their uncertainty analysis for e.g. the R-test [39, 40], the probing test [31] and the machining test [6]. The contributors 3 and 4 are present only in machining tests. The objective of this section is to present experimental assessment of the uncertainty in the measured geometry of the finished test piece and its propagation to the identified machine geometric errors.

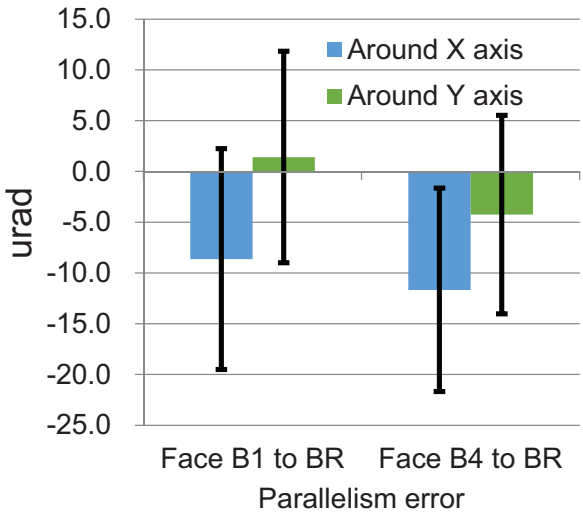

Figure 11: The error bars show the assessed uncertainty ($k = 1$) in the estimated parallelism error of the face B_1 to B_R (left) ($\Delta a_{B1,BR}$ around the X-axis, and $\Delta b_{B1,BR}$ around the Y-axis), and that of B_4 to B_R (right) ($\Delta a_{B4,BR}$ around X and $\Delta b_{B4,BR}$ around Y). The columns show the estimated values shown in Table 1 #2 and #12.

5.2. Uncertainty assessment procedure and results

Each geometric error of the finished test piece shown in Table 1 was calculated by fitting a set of points measured by a CMM by a circle or a plane. For example, the parallelism error of the face B_1 to B_R, $\Delta a_{B1,BR}$ and $\Delta b_{B1,BR}$ in Table 1 #2, is calculated by measuring 16 points on both faces, and then fitting them by a plane, whose orientations define $\Delta a_{B1,BR}$ and $\Delta b_{B1,BR}$. Each measured point contains some variation caused by uncertainty contributors discussed above. Its propagation to the uncertainty in $\Delta a_{B1,BR}$ is assessed as follows: take three points randomly from 16 points and calculate parallelism errors, $\Delta a_{B1,BR}$ and $\Delta b_{B1,BR}$. Repeat this for many other combinations of points, and the standard deviation of the calculated set of $\Delta a_{B1,BR}$ ($\Delta b_{B1,BR}$) is regarded as the uncertainty in $\Delta a_{B1,BR}$ ($\Delta b_{B1,BR}$)

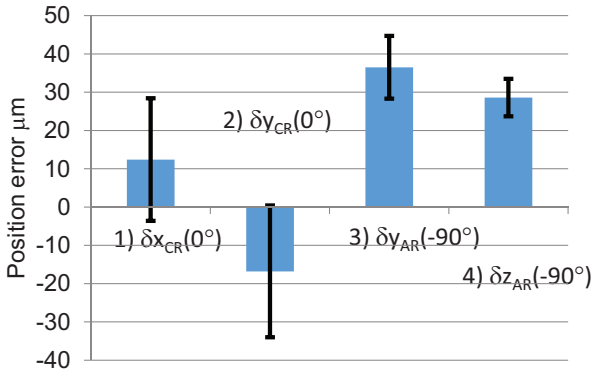

a)

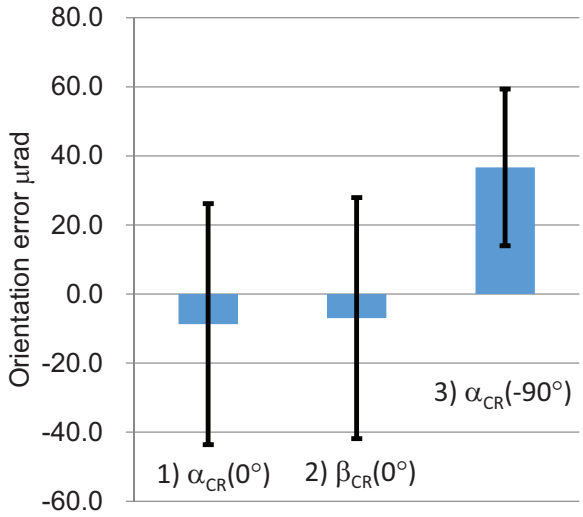

b)

Figure 12: The error bars represent the uncertainty ($k = 1$) in the estimated machine geometric errors shown in Table 2. The blue bars shows the estimates from the machining test (Table 2 ("Estimated from finished test piece")).

(the coverage factor $k = 1$). Figure 11 shows the assessed uncertainty in $\Delta a_{B1,BR}$ and $\Delta b_{B1,BR}$ in error bars, as well as that in $\Delta a_{B4,BR}$ and $\Delta b_{B4,BR}$. The uncertainty in all the geometric errors shown in Table 1 is assessed analogously.

Then, their propagation to the combined uncertainty in the identified machine geometric errors, shown in Table 2, can be assessed by applying the standard statistical uncertainty analysis procedure [41] to Eqs. (10) to (21). Figure 12 (error bars) shows the assessed uncertainties ($k = 1$) in estimated position and orientation errors of C-axis. It should be noticed that the estimated value of some parameters, e.g. $\delta x_{CR}(0^\circ)$, $\delta y_{CR}(0^\circ)$, $\alpha_{CR}(0^\circ)$ and $\beta_{CR}(0^\circ)$, is not significantly large compared to the assessed uncertainty.

6. Conclusion

This paper proposed a machining test containing features finished by a turning operation by a rotary table, which is indexed either horizontal ($A = 0^\circ$) or vertical ($A = -90^\circ$) by a swiveling axis. The relationship between the geometric errors of the finished test piece to position and orientation errors of the rotary table's axis average line is formulated. Based on this formulation, 1) position and orientation errors of the rotary table's axis average line at both $A = 0^\circ$ and -90°, 2) squareness errors of linear axes, and 3) the rotary table's radial and axial error motions at both $A = 0^\circ$ and -90°, can be observed from the finished test piece's geometric errors measured by using a CMM.

Experimental demonstration was presented. The rotary axis geometric errors identified from the finished test piece's geometry were compared

with those estimated by a conventional error calibration test using a touch-triggered probe and a precision sphere. The difference was larger in some errors, e.g. the X-position error of C-axis average line at $A = 0°$ was different by about 18 μm. This can be due to the thermal influence, since the probing test can be performed only when the rotary table (and the spindle) was not rotating, and thus it may not show the machine's geometric errors in actual machining operations.

On the other hand, a potential issue with a machining test is the uncertainty caused by the variation due to the machining process (cutting forces) and CMM measurement on a machined surface. As a part of uncertainty contributors, the influence of the variation in the measured geometric errors of the finished test piece was assessed.

References

[1] `https://www.rolls-royce.com/products` (viewed on June 20, 2018).

[2] ISO 230-1:2012, Test code for machine tools – Part 1: Geometric accuracy of machines operating under no-load or quasi-static conditions.

[3] ISO 230-7:2006, Test Code for Machine Tools – Part 7: Geometric Accuracy of Axes of Rotation.

[4] J. Mayr, J. Jedrzejewski, E. Uhlmann, A. Donmez, W. Knapp, F. H artig, K. Wendt, T. Moriwaki, P. Shore, R. Schmitt, C. Brecher, T. Wuerz, K. Wegener, Thermal issues in machine tools, CIRP Ann. - Manuf. Technol., 61(2) (2012) 771–791.

[5] M. Gebhardt, J. Mayr, N. Furrer, T. Widmer, S. Weikert, W. Knapp W (2014) High Precision Grey-Box Model for Compensation of Thermal Errors on 5-Axis Machine Tools. CIRP Annals – Manufacturing Technology 63(1):509-512.

[6] Ibaraki S, Ota Y (2014) A machining test to calibrate rotary axis error motions of five-axis machine tools and its application to thermal deformation test, International Journal of Machine Tools and Manufacture, 86, 81-88.

[7] Schwenke H, Knapp W, Haitjema H, Weckenmann A, Schmitt R, Delbressine F (2008) Geometric Error Measurement and Compensation of Machines – An Update. CIRP Annals – Manufacturing Technology 2008; 57(2):560-575.

[8] Ibaraki S, Knapp W, Indirect Measurement of Volumetric Accuracy for Three-axis and Five-axis Machine Tools: A Review, International Journal of Automation Technology 2012; 6 (2):110-124.

[9] ISO 10791-1:2015, Test conditions for machining centres – Part 1: Geometric tests for machines with horizontal spindle (horizontal Z-axis)

[10] ISO 10791-6:2014, Test conditions for machining centers – Part 6: Accuracy of speeds and interpolations.

[11] ISO 10791-7:2015, Test conditions for machining centres – Part 7: Accuracy of a finished test piece.

[12] NAS979:1969, Uniform Cutting Test – NAS Series, Metal Cutting Equipment Specifications, 34-37.

[13] Bossoni S, Cupic J, Test piece for simultaneous 5-axis machining, Laser metrology and machine performance VIII; 2007; 24-33.

[14] Hong C, Ibaraki S, Matsubara A, Influence of position-dependent geometric errors of rotary axes on a machining test of cone frustum by five-axis machine tools, Precision Engineering; 2011; 35(1):1-11.

[15] Jiang Z, Ding J, Song Z, Modeling and simulation of surface morphology abnormality of 'S' test piece machined by five-axis CNC machine tool, International Journal of Advanced Manufacturing Technology; 2015: 1-15

[16] `http://www.ncg.de`

[17] Ohta K, Li Z, Tsutsumi M, Proposal of a Machining Test of Five-Axis Machining Centers Using a Truncated Square Pyramid, Key Engineering Materials; 2012; 523-524: 475-480.

[18] Hasegawa S, Sato R, Shirase K, Influences of geometric and dynamic synchronous errors onto machined surface in 5-axis machining center, Journal of Advanced Mechanical Design, Systems, and Manufacturing; 2016; 10(5): JAMDSM0071.

[19] Ibaraki S, Tsujimoto S, Nagai Y, Sakai Y, Morimoto S, Miyazaki Y, A pyramid-shaped machining test to identify rotary axis error motions on five-axis machine tools: Software development and a case study, International Journal of Advanced Manufacturing Technology; 2017.

[20] Lin P, Tzeng C (2008) Modeling and measurement of active parameters

and workpiece home position of a multi-axis machine tool, International Journal of Machine Tools and Manufacture, 48-3/4, 338-349.

[21] Bono M, Kroll J (2008) Tool setting on a B-axis rotary table of a precision lathe, Int'l J. of Machine Tools and Manufacture, 48(11), 1261-1267.

[22] Velenosi A, Campatelli G, Scippa A (2015) Axis geometrical errors analysis through a performance test to evaluate kinematic error in a five axis tilting-rotary table machine tool, Precision Engineering, 39, 224-233.

[23] Morimoto Y, Nakato K, Gontani M, Accuracy Evaluation of 5-Axis Machining Center Based on Measurements of Machined Workpiece – Evaluation of Accuracy of 5-Axis Controlled Machining Center –, International Journal of Automation Technology; 2012; 6(5): 675-68.

[24] ISO 13041-6: 2009, Test conditions for numerically controlled turning machines and turning centres – Part 6: Accuracy of a finished test piece.

[25] ISO 1708: 1989, Acceptance conditions for general purpose parallel lathes – Testing of the accuracy.

[26] ISO 841:2001, Industrial automation systems and integration – Numerical control of machines – Coordinate system and motion nomenclature.

[27] ISO 1101:2017, Geometrical product specifications (GPS) – Geometrical tolerancing – Tolerances of form, orientation, location and run-out.

[28] Abbaszaheh-Mir Y, Mayer JRR, Clotier G, Fortin C (2002) Theory and simulation for the identification of the link geometric errors for a five-

axis machine tool using a telescoping magnetic ball-bar, International Journal of Production Research, 40(18): 4781–4797.

[29] Inasaki I, Kishinami K, Sakamoto S, Sugimura N, Takeuchi Y, Tanaka F (1997) Shaper generation theory of machine tools – its basis and applications, Yokendo, Tokyo (in Japanese).

[30] S. Ibaraki, T. Iritani, T. Matsushita, Calibration of location errors of rotary axes on five-axis machine tools by on-the-machine measurement using a touch-trigger probe, Int. J. Mach. Tools Manuf, 58 (2012) 44-53.

[31] S. Ibaraki, T. Iritani, T. Matsushita, Error map construction for rotary axes on five-axis machine tools by on-the-machine measurement using a touch-trigger probe, Int. J. Mach. Tools Manuf, 68 (2013) 21-29.

[32] S. Ibaraki, Yusuke Ota, Error Calibration for Five-Axis Machine Tools by On-the-Machine Measurement Using a Touch-Trigger Probe, International Journal of Automation Technology, 8(1) (2014) 20-27.

[33] JRR Mayer, Five-axis machine tool calibration by probing a scale enriched reconfigurable uncalibrated master balls artefact, CIRP Ann. - Manuf. Technol. 61(1) (2012) 515-518.

[34] Z. Jiang, B. Song, X. Zhou, X. Tang, S. Zheng, Single setup identification of component errors for rotary axes on five-axis machine tools based on pre-layout of target points and shift of measuring reference, Int. J. Mach. Tools Manuf, 98 (2015) 1-11.

[35] S. Weikert S, R-test; a new device for accuracy measurements on five axis machine tools, CIRP Ann. - Manuf. Technol. 53(1) (2004) 429-432.

[36] S. Ibaraki, Y. Nagai, H. Otsubo, Y. Sakai, S. Morimoto, Y. Miyazaki, R-Test Analysis Software for Error Calibration of Five-Axis Machine Tools –Application to a Five-Axis Machine Tool with Two Rotary Axes on the Tool Side–, International Journal of Automation Technology, 9(4) (2015) 387-395.

[37] S. Ibaraki, C. Oyama, H. Otsubo, Construction of an error map of rotary axes on a five-axis machining center by static R-test, Int. J. Mach. Tools Manuf, 51 (2011) 190-200.

[38] P. Hernández Becerro, P. Blaser, J. Mayr, S. Weikert, K. Wegener, Measurement of the effect of the cutting fluid on the thermal response of a five-axis machine tool, Laser Metrology and Machine Performance XII, (2017)

[39] B. Bringmann, W. Knapp, Machine tool calibration: Geometric test uncertainty depends on machine tool performance, Precision Engineering, 33 (2009) 524–529.

[40] B. Bringmann, J. P. Besuchet, L. Rohr, Systematic evaluation of calibration methods, CIRP Ann. - Manuf. Technol. 57 (2008) 529-532.

[41] JCGM 100:2008, Evaluation of measurement data – Guide to the expression of uncertainty in measurement (GUM), 2008.